Meteoritics & Planetary Science 40, Nr 6, 917–932 (2005)
Abstract available online at http://meteoritics.org

Small Antarctic micrometeorites: A mineralogical and in situ oxygen isotope study

Matthieu GOUNELLE[1, 2, 3*], Cécile ENGRAND[1, 5], Michel MAURETTE[1], Gero KURAT[4], Kevin D. McKEEGAN[5], and Franz BRANDSTÄTTER[4]

[1]CSNSM, Bâtiment 104, 91 405 Orsay Campus, France
[2]Université Paris XI, Bâtiment 104, 91 405 Orsay Campus, France
[3]Department of Mineralogy, The Natural History Museum, London SW7 5BD, UK
[4]Mineralogish-Petrographische Abteilung, Naturhistorisches Museum, Postfach 417, A-1014 Wien, Austria
[5]Department of Earth and Space Sciences, University of California—Los Angeles, Los Angeles, California 90095–1567, USA
[*]Corresponding author. E-mail: gounelle@csnsm.in2p3.fr

(Received 15 December 2004; revision accepted 05 April 2005)

Abstract–We have investigated the texture, bulk chemistry, mineralogy, as well as the anhydrous minerals oxygen isotopic composition of 67 small Antarctic micrometeorites (AMMs) collected at Cap Prudhomme, Antarctica, and belonging to the currently poorly studied size fraction 25–50 μm. When compared to larger (50–400 μm) micrometeorites collected at the same site in Antarctica with the same techniques, no significant differences are found between the two populations. We therefore conclude that the population of Cap Prudhomme AMMs is homogeneous over the size range 25–400 μm. In contrast, small AMMs have different textures, mineralogy, and oxygen isotopic compositions than those of stratospheric interplanetary dust particles (IDPs). Because small AMMs (<50 μm) overlap in size with IDPs, the differences between these two important sources of micrometeorites can no longer be attributed to a variation of the micrometeorite composition with size. Physical biases introduced by the collection procedures might account for these differences.

INTRODUCTION

Micrometeorites with sizes <1 mm account for most of the extraterrestrial matter accreting to Earth at present (Love and Brownlee 1993). Micrometeorites are a different and potentially more representative sample of the asteroid belt than meteorites, mainly because their dynamic evolution is controlled by Poynting-Robertson drag (Kortenkamp et al. 2001), as opposed to the conjunction of the Yarkovsky effect and orbital resonances with giant planets for meteorites (Vokrouhlicky and Farinella 2000). Prior to sample return from missions such as Stardust, which will bring back dust from comet Wild 2, and Hayabusa, which will sample the asteroid Itokawa, the main available micrometeorite sources are the polar ice caps and the stratosphere. Stratospheric interplanetary dust particles (IDPs) have been systematically collected by NASA at altitudes of ~20 km since 1981 (Brownlee 1985). Polar micrometeorites were first collected in the Greenland ice cap (e.g., Maurette et al. 1986). More recently, large numbers of micrometeorites have been collected in Antarctica in the blue ice fields of Terre Adélie, at Cap Prudhomme (e.g., Maurette et al. 1991) and at the nearby Astrolabe glacier (Gounelle et al. 1999), as well as at Yamato mountains (e.g., Terada et al. 2001). Water wells have provided micrometeorites at South Pole (Taylor et al. 1998), and at Dome Fuji (Nakamura et al. 1999). Recently Duprat et al. (2003) have collected micrometeorites in the surface snow in the Antarctic central regions (station CONCORDIA, Dome C).

All micrometeorite collections use complex procedures to recover relatively uncontaminated submillimeter dust from a diversity of environments. Different techniques are used for each environment, resulting in collections with their own characteristics, in terms of the number and nature of particles recovered. The differences are especially striking between Antarctic micrometeorites (AMMs) collected in blue ice (such as Cap Prudhomme) and the IDPs collected in the stratosphere. While IDPs are captured by using silicone oil-coated collectors attached on the wings of NASA U2 and ER2 stratospheric aircraft (Warren and Zolensky 1994), Cap Prudhomme micrometeorites are extracted from the blue ice after a procedure involving 1) melting blue ice with a steam

Table 1. Textural types of micrometeorites in the size fraction 25–50 μm. Xtal, fg, sc, and cs stand for crystalline, fine-grained, and scoriaceous micrometeorites, respectively.

Textural type	xtal	fg	sc	cs
Number of particles	10	42	8	7
Percentage relative to the extraterrestrial matter	15	63	12	10

generator, 2) mechanical pumping of the melt water, and 3) filtering of the water using three different mesh sizes: 25–50 μm, 50–100 μm, and 100–400 μm (Maurette et al. 1991). This results in Cap Prudhomme AMMs belonging to the size range of 25–400 μm, whereas IDPs are smaller than 50 μm (Rietmeijer 1998).

AMMs with sizes larger than 50 μm are very different from IDPs in terms of morphology and mineralogy (Engrand and Maurette 1998; Kurat et al. 1994b). For example, AMMs lack anhydrous chondritic porous particles, and often exhibit large isotopic anomalies (Messenger 2000), or hypothesized interstellar components, such as glass embedded with metal and sulfides (GEMS) (Bradley 1994; Bradley et al. 1999). Carbonates and sulfides, commonly found in IDPs (Tomeoka and Buseck 1985; Zolensky and Thomas 1995) are absent or rare in the Cap Prudomme AMMs collection (Duprat et al. 2003; Engrand and Maurette 1998).

Differences between AMMs and IDPs might be due to collection biases, to a temporal change in the composition of the micrometeorite flux onto the Earth, or to a variation of the micrometeorite composition with size. The latter possibility is strengthened by the fact that the numerous differences between micrometeorites (both stratospheric and polar) and meteorites indicate that the composition of extraterrestrial matter does indeed vary with size (Engrand and Maurette 1998; Rietmeijer 1998).

The goals of this paper are threefold. First, we want to characterize the morphology, bulk chemistry, mineralogy, and anhydrous grains oxygen isotopic composition of AMMs belonging to the small size fraction (25–50 μm), providing a large data set for samples described so far in only one abstract (Maurette et al. 1992b). Second, we will compare small AMMs with larger AMMs (50–400 mm), also collected at Cap Prudhomme. This comparison will enable us to assess if the AMMs population is homogeneous within the whole size range 25–400 μm, independently of collection biases. Third, because the 25–50 μm AMMs overlap in size with the largest IDPs, we will be able to directly compare AMMs and IDPs. This is an important step in understanding if the differences observed between large AMMs and IDPs can be ascribed to a size bias or is due to other causes.

SAMPLES AND INSTRUMENTAL METHODS

386 particles with sizes between 25 and 50 μm and that were collected at Cap Prudhomme during the 1991 field season (Maurette et al. 1992a) were first optically selected for their black color and irregular surface, and then were embedded in epoxy and polished. Broad selection criteria were used to ensure that no unusual extraterrestrial particle was missed. These particles were studied at the Vienna Naturhistorisches Museum with a scanning electron microscope (SEM) JEOL JSM-6400 run at 15 keV and equipped with a KEVEX energy dispersive X-ray (EDX) analysis system. Micrometeorites were identified from their chondritic EDX spectrum. Backscattered electron images (BSE) of selected micrometeorites were then taken with a PHILIPS XL 40 field emission gun scanning electron microscope at ONERA (Chatillon, France). The mineral grains and matrix of micrometeorites were analyzed using a SX100 CAMECA electron microprobe (EMP) operated at 15 kV with a beam current of 20 nA (Vienna University), and with a CAMEBAX EMP operated at 15 kV with a beam current of 10 nA (Paris University). All these analyses were performed using a focused beam with a diameter of ~1 μm. Bulk chemistry was determined with a SX100 CAMECA electron microprobe operated at 15 keV and 40 nA (Paris University), with a defocused beam ~30 μm. Detection limits are around 0.02 wt% for all elements. Natural as well as synthetic standards were used; data were corrected using the PAP Cameca program.

The oxygen isotopic composition of anhydrous minerals was determined with the UCLA CAMECA IMS 1270 following the procedures previously used for the analyses of larger micrometeorites (Engrand et al. 1999a). Data are expressed in the usual delta (per mil) unit, relative to the standard mean ocean water (SMOW). The precision of the analyses was of the order of ~1‰ for both $\delta^{17}O_{SMOW}$ and $\delta^{18}O_{SMOW}$. For the sake of simplicity, we will drop the index SMOW throughout this paper. Pyroxene and olivine analyses were corrected for matrix effect using the San Carlos olivine standard. Analyses of an enstatite standard under our experimental conditions show that relative variations of instrumental mass fractionation compared to San Carlos olivine are <1‰/amu.

RESULTS

Texture

Sixty-seven particles with an EDX spectrum compatible with a chondritic composition were found among the 386 particles. Micrometeorites were found to belong to the four textural types (Table 1) previously described by Kurat et al. (1994b): 10 crystalline AMMs consisting of an assemblage of anhydrous silicates (olivine and pyroxene), 42 fine-grained AMMs consisting of a phyllosilicate-rich matrix supporting olivine, pyroxene and accessory minerals, 8 scoriaceous AMMs consisting of a highly vesicular melt which contain

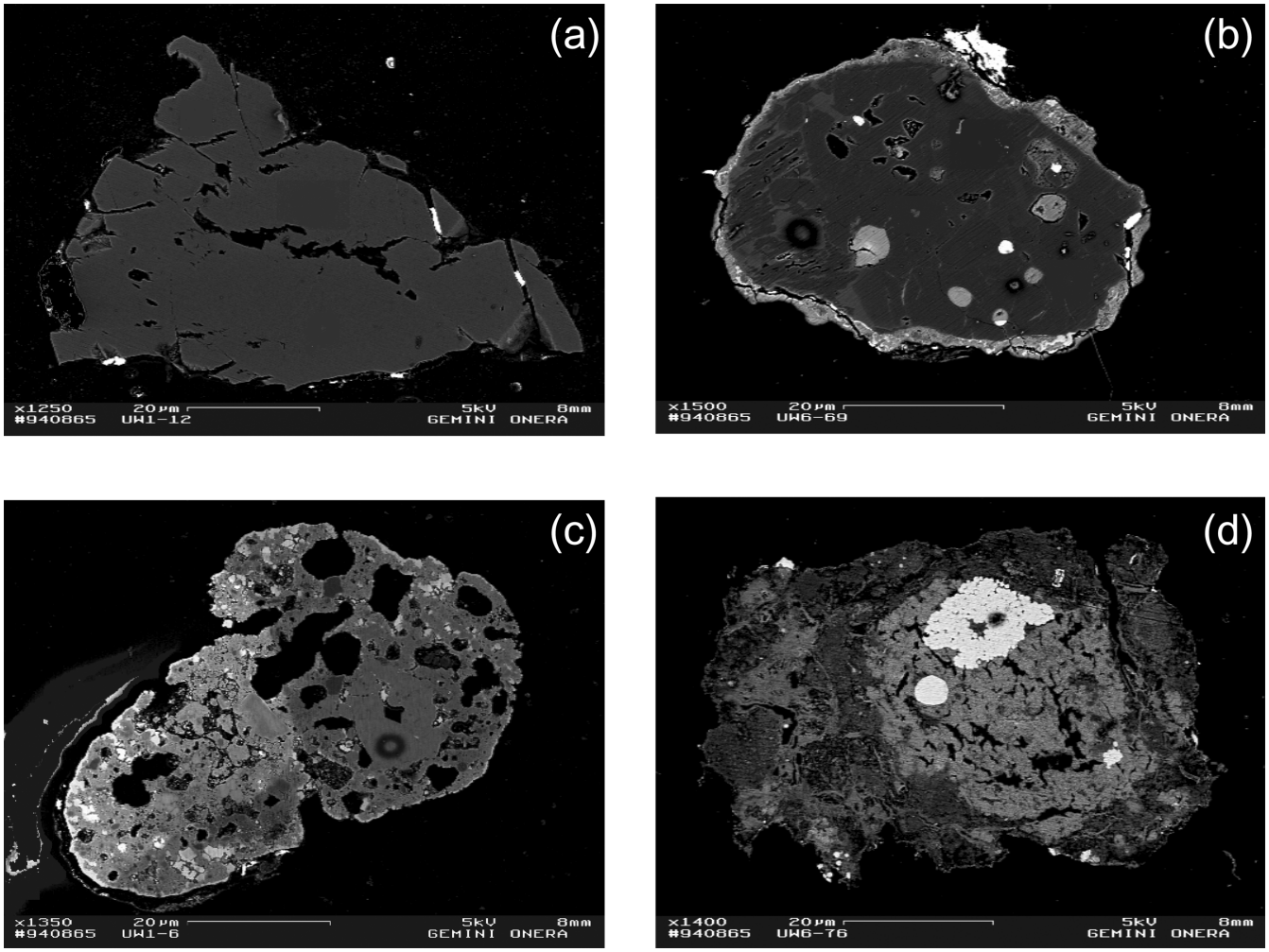

Fig. 1. Backscattered scanning electron images of 25–50 μm AMMs observed in polished sections: a) Crystalline micrometeorite with irregular morphology; b) Crystalline micrometeorite with round morphology; c) Scoriaceous micrometeorite; d) Fine-grained micrometeorite with magnetite framboids.

rare relic phases (olivine or pyroxene) (Fig. 1), and 7 cosmic spherules consisting of glass, olivine and magnetite assemblages. Both crystalline and fine-grained AMMs are considered as unmelted (UMMs) micrometeorites, contrary to scoriaceous micrometeorites and cosmic spherules that are partially and fully melted, respectively (Engrand and Maurette 1998).

Crystalline AMMs have morphologies varying from irregular to round (Fig. 1). Usually, irregular particles consist of a monocrystal, are highly cracked, and show no magnetite rim. Conversely, round grains display complex textures, e.g., porphyritic and poikilitic, and have a magnetite rim that is either discontinuous or completely surrounds the particle. Fine-grained AMMs have morphologies varying from irregular to round with a discontinuous to complete magnetite rim coating the external surface (Fig. 1). Scoriaceous AMMs have round to oval morphologies (Fig. 1), and most of them are coated with a magnetite rim either complete or discontinuous. Four cosmic spherules have perfectly round morphologies, two exhibit circular voids indicating the probable loss of a Fe-Ni nugget (Taylor et al. 2000), while one is broken. Magnetite rim appears in three spherules out of four.

Bulk Chemistry

The bulk chemistry of 38 randomly selected particles was determined using EMP with a defocused beam of approximately 30 μm. The bulk chemical compositions are reported in the Appendix and presented in Fig. 2 in the form of an atomic ternary diagram Mg-Fe-Si. Crystalline micrometeorites are very enriched in magnesium compared to fine-grained AMMs and scoriaceous micrometeorites. Fine-grained micrometeorites have varying compositions from very Mg-rich to very Fe-rich. Scoriaceous micrometeorites (with the exception of UW6-29) compositions overlap with fine-grained AMMs compositions. Cosmic spherules have a

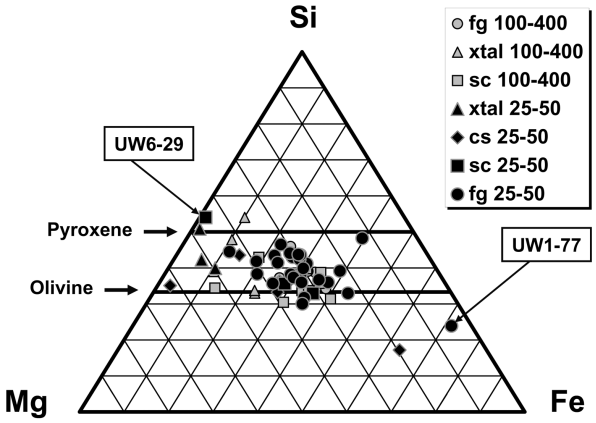

Fig. 2. An atomic ternary diagram (Si-Fe-Mg) showing the bulk compositions of small micrometeorites (data in the Appendix). A comparison is made with the bulk compositions of the large AMMs (Kurat et al. 1994) measured with the same technique (EMP defocused beam). The pyroxene and the olivine solid solutions are shown as solid lines.

very wide range of compositions, from very Fe-poor (UW1-66) to very iron-rich (UW1-28).

Mineralogy and Mineral Chemistry

Crystalline AMMs consist mainly of olivine and pyroxene set in a glass of feldspathic composition; accessory minerals are poorly defined iron oxyhydroxides, Fe-Ni metal, magnetite and low-Ni sulfides (very rare). Pyroxene is the most abundant mineral in crystalline AMMs (see Table 2 for compositions). Low-Ca pyroxenes are fairly iron-poor (0.91–6.82 wt% FeO) and have a highly variable CaO content (0.27–2.12 wt%). One pigeonite grain ($En_{91}Wo_6$) associated with iron-poor olivine (Fo_{97}) and one augite grain ($En_{54}Wo_2$) have been found. The pigeonite has a high Cr_2O_3 content (1.33 wt%) and a low FeO/MnO ratio (~3), whereas the augite has a moderate Cr_2O_3 content (0.53 wt%) and an intermediate FeO/MnO ratio (~38). Olivine is the second most abundant mineral in crystalline micrometeorites (see Table 3 for compositions). Most of the olivines are iron-rich (Fa_{15}–Fa_{36}), except for UW6-69, which has a forsteritic composition (Fo_{97}). All olivines are poor in Ni (NiO < 0.06 wt%) regardless of their iron content. The FeO/MnO ratio ranges from 60 to 80 for the iron-rich olivines and equals 10 for the forsteritic one. The CaO content is intermediary and varies between 0.10 and 0.39 wt%. The Cr_2O_3 content is highly variable (0.09–0.71 wt%), with the high chromium content corresponding to the forsteritic olivine. The Al_2O_3 content varies between 0.03 and 0.20 wt%. Accessory phases are usually too small for electron microprobe analyses. Magnetite is common in some particles as a thin (~1 μm) discontinuous or complete rim (Table 1 and Fig. 1). Iron oxyhydroxide occurs in voids and close to the particle surface. Low-Ni metal is enclosed in pyroxenes of variable composition ($En_{86}Wo_4$–$En_{98}Wo_1$). One low-Ni iron sulfide has been found.

Fine-grained AMMs consist of a fine-grained matrix supporting isolated pyroxene and olivine grains, magnetite, low-Ni iron sulfides, chromite, metal, and iron oxyhydroxides. The composition of matrix together with its variable EMP analysis totals (Table 4) suggests that it consists mainly of dehydrated phyllosilicates with a wide range of compositions and minor iron-nickel sulfides. Low-Ca pyroxene grains are the most abundant grains isolated in the matrix of fine-grained AMMs (see Table 2 for compositions). A predominant population has enstatitic compositions ($En_{94–99}Wo_3$) and a minor population is more iron-rich ($En_{84}Wo_0$). The CaO content ranges from 0.25 to 1.85 wt%. The FeO/MnO ratio ranges from 4 to 29. The Cr_2O_3 and TiO_2 contents are intermediate (0.09–1.00 wt% and 0.04–0.17 wt%, respectively) except for the iron-rich pyroxene ($En_{82}Wo_2$) that has a high TiO_2 content (0.64 wt%). One pigeonite was found; it has a low FeO/MnO ratio (~11) and a high Al_2O_3 content (4.05 wt%). Most of the olivines have (see Table 3 for compositions) a high iron content ($Fo_{78–82}$), while one is iron-poor (Fo_{97}). They have intermediary minor elements contents (Cr_2O_3 0.04–0.84 wt% and TiO_2 below 0.07 wt%), and their FeO/MnO ratio varies from 12 to 68. Accessory minerals are more abundant in fine-grained AMMs than in crystalline AMMs. Magnetite, besides being common as a rim at particle surface, often occurs as loose, subhedral grains in the matrix. A few Mg-rich magnetite grains have been found both in the matrix and in the rim. A magnetite rich in titanium (10.4 wt% TiO_2) has been found on the side of a particle associated with a magnetite of pure composition. Magnetite framboids have been found in the matrix of two fine-grained AMMs (Fig. 3). A Mg-phosphate has been found, but was too small to be analyzed with the electron microprobe. Because this grain is located in a particle void, it could be of terrestrial origin. Low-Ni iron sulfides, chromite, Fe-Ni metal, and iron oxyhydroxides (all rare) have been found in the matrix.

Scoriaceous small AMMs are dominated by glass, quenched olivine and quench magnetite—all too fine-grained to allow EMPA analysis. Accessory minerals, also very fine-grained, are low-Ni sulfides and chromium-rich magnetite. Very few relic grains have been found: just one fayalitic olivine (Fo_{63}) and one iron-poor low-Ca pyroxene ($En_{99}Wo_0$). The olivine has a quite high FeO/MnO ratio (~68) and is fairly poor in minor elements (except for CaO = 0.3 wt%). The pyroxene has a quite low FeO/MnO ratio (~11), is fairly poor in minor elements, and has a CaO content compatible with an orthopyroxene composition (0.13 wt%).

Cosmic spherules are dominated by glass, pyroxene, olivine, and magnetite. Most minerals are too small to provide reliable EMP data. The olivine (Table 3) is iron-rich ($Fo_{57–62}$). The glass is depleted in K_2O and Na_2O and has a high Ca content (Table 4).

Table 2. Analyses of pyroxenes from micrometeorites belonging to the 25–50 μm size fraction. Data in wt%. Xtal, fg, and sc stand for crystalline, fine-grained, and scoriaceous micrometeorites, respectively. B.d. stands for below detection limit.

Micrometeorite	UW1-12	UW6-74	UW5-93	UW6-69	UW3-56	UW6-53	UW6-53	UW1-44	UW6-29	UW5-104	UW5-104
Textural type	xtal	xtal	xtal	xtal	xtal	xtal	xtal	xtal	sc	fg	fg
SiO_2	58.8	55.1	52.3	56.6	55.8	58.5	58.2	57.6	59.1	56.0	58.1
TiO_2	0.03	0.22	0.26	0.12	0.17	0.10	0.11	0.09	0.04	0.11	0.08
Al_2O_3	0.31	1.65	1.17	1.23	1.38	0.66	0.63	0.96	0.15	1.44	0.46
Cr_2O_3	0.6	0.99	0.53	1.33	0.81	0.59	0.63	1.15	0.35	1.04	0.76
FeO	1.91	6.82	10.9	1.72	4.44	0.91	2.02	2.06	0.78	4.09	1.74
MnO	0.09	0.58	0.29	0.6	0.72	0.09	0.10	0.46	0.07	0.37	0.49
MgO	38.9	32.5	18.7	34.9	34.4	39.4	38.2	37.0	40.4	35.1	38.0
NiO	b.d.	b.d.	b.d.	b.d.	b.d.	b.d.	0.05	b.d.	b.d.	b.d.	b.d.
CaO	0.27	2.12	13.7	3.31	1.34	0.55	0.60	1.28	0.13	1.39	0.67
Na_2O	b.d.	b.d.	0.67	0.04	0.07	b.d.	b.d.	b.d.	b.d.	0.03	b.d.
K_2O	b.d.	b.d.	b.d.	0.03	b.d.	b.d.	b.d.	b.d.	b.d.	b.d.	b.d.
Total	100.91	99.98	98.52	99.88	99.12	100.79	100.53	100.61	101.02	99.57	100.32

Micrometeorite	UW5-104	UW5-104	UW6-12	UW1-69	UW3-23	UW6-18	UW5-62	UW6-85	UW6-55	UW5-93
Textural type	fg	fg	fg	fg	fg	fg	fg	fg	fg	fg
SiO_2	56.0	58.1	58.2	58.6	57.4	57.3	58.6	54.3	53.0	52.6
TiO_2	0.11	0.08	0.04	0.09	0.17	0.14	0.08	0.64	0.28	0.07
Al_2O_3	1.44	0.46	0.33	0.48	1.48	0.83	0.65	0.87	4.05	0.98
Cr_2O_3	1.04	0.76	0.69	0.60	1.00	0.53	0.67	0.45	1.31	0.78
FeO	4.09	1.74	3.63	1.29	2.12	2.33	0.63	11.1	7.3	4.26
MnO	0.37	0.49	0.13	0.17	0.55	0.11	0.21	0.51	0.62	0.26
MgO	35.1	38.0	37.4	39.0	36.2	38.0	39.0	30.9	29.6	38.7
NiO	b.d.	b.d.	b.d.	b.d.	b.d.	0.13	b.d.	b.d.	0.03	b.d.
CaO	1.39	0.67	0.25	0.57	1.85	0.62	0.63	0.82	3.1	1.29
Na_2O	0.03	b.d.	b.d.	b.d.	b.d.	b.d.	0.04	b.d.	b.d.	b.d.
K_2O	b.d.	b.d.	b.d.	b.d.	b.d.	b.d.	b.d.	b.d.	0.03	b.d.
Total	99.57	100.32	100.67	100.79	100.77	99.98	100.51	99.59	99.32	98.94

Table 3. Analyses of olivines from micrometeorites belonging to the 25–50 μm size fraction. Data in wt%. Xtal, fg, and sc stand for crystalline, fine-grained, and scoriaceous micrometeorites respectively. B.d. stands for below detection limit.

Micrometeorite	UW1-06	UW5-93	UW6-69	UW6-88	UW6-88	UW6-85	UW6-55	UW3-04	UW6-85	UW1-66
Textural type	sc	xtal	xtal	xtal	xtal	fg	fg	fg	fg	cs
SiO_2	35.8	35.2	41.1	37.9	39.1	38.7	40.6	41.3	37.7	35
TiO_2	b.d.	b.d.	0.04	b.d.	b.d.	0.05	0.03	b.d.	0.07	0.08
Al_2O_3	0.04	b.d.	0.2	0.13	0.06	b.d.	0.04	0.04	0.17	0.48
Cr_2O_3	0.09	0.09	0.71	0.47	0.26	0.04	0.31	0.76	0.83	0.46
FeO	32	31.7	2.5	19.8	14.04	16.7	11.4	2.84	19.9	32.1
MnO	0.47	0.4	0.24	0.29	0.22	0.43	0.67	0.23	0.39	0.22
MgO	30	31.4	54.1	40.5	45.6	43.2	45.8	54.7	39	29.3
NiO	b.d.	b.d.	b.d.	0.06	0.03	b.d.	b.d.	b.d.	0.14	0.06
CaO	0.31	0.25	0.39	0.12	0.1	b.d.	0.16	0.19	0.08	0.47
Na_2O	0.08	b.d.	b.d.	b.d.	b.d.	b.d.	b.d.	b.d.	b.d.	b.d.
K_2O	b.d.	b.d.	b.d.	b.d.	b.d.	b.d.	b.d.	b.d.	b.d.	b.d.
Total	98.79	99.04	99.28	99.27	99.41	99.12	99.01	100.06	98.28	98.21

Table 4. Representative analyses of matrix of fine-grained micrometeorites and glass of cosmic spherules. Data in wt%. Xtal, fg, sc, and cs stand for crystalline, fine-grained, scoriaceous, and cosmic spherules, respectively. B.d. stands for below detection limit. N.a. stands for non-analyzed.

Micrometeorite	UW1-03	UW1-03	UW1-74	UW3-03	UW3-28	UW5-96	UW5-104	UW3-25	UW6-92
Textural type	fg	fg	fg	fg	fg	fg	fg	cs	cs
SiO_2	30.3	37.7	39.3	27.1	27.3	35.6	33.3	47.9	38.6
TiO_2	0.11	0.09	0.19	0.11	0.06	0.13	0.1	0.23	0.13
Al_2O_3	3.36	1.65	2.55	2.71	3.25	2.43	2.71	3.01	3.93
Cr_2O_3	0.26	0.46	0.62	0.3	0.12	0.53	0.46	b.d.	b.d.
FeO	45.1	29.1	24.8	47.3	44.5	35.8	35.4	19.4	24.3
MnO	0.26	0.29	0.44	0.25	0.23	0.07	0.14	0.62	0.22
MgO	14.1	22.8	18.8	13.9	17.4	6.81	11.6	20.1	29.7
NiO	0.11	0.11	0.14	0.07	0.22	0.08	0.22	0.04	b.d.
CaO	1.13	0.55	0.85	0.1	0.59	0.4	0.4	5.18	1.25
Na_2O	0.2	0.16	0.58	0.05	0.03	0.54	0.51	b.d.	b.d.
K_2O	0.14	0.21	0.16	b.d.	b.d.	0.45	0.13	b.d.	b.d.
P_2O_5	0.14	0.28	b.d.	0.22	0.08	b.d.	b.d.	n.a.	n.a.
S	0.14	0.17	0.31	0.07	0.08	0.3	0.42	n.a.	n.a.
Total	95.35	93.57	88.74	92.18	93.86	83.14	85.39	96.46	98.27

The Oxygen Isotopic Composition of Anhydrous Minerals

The oxygen isotopic compositions of pyroxenes and olivines belonging to 8 crystalline, 5 fine-grained, and 1 scoriaceous micrometeorite are reported in Table 5 and shown on a three-isotope diagram in Fig. 4.

For olivine and pyroxene grains from crystalline micrometeorites, $\delta^{18}O$ varies from −11.0 to 1.0‰ and $\delta^{17}O$ varies from −11.7 to −0.80‰, respectively. For olivines and pyroxenes from fine-grained micrometeorites, $\delta^{18}O$ varies from −4.1 to 2.5‰ and $\delta^{17}O$ varies from −4.9 to 2.3‰, respectively. A single pyroxene grain large enough to be measured in a scoriaceous micrometeorite has $\delta^{18}O = 8.5 \pm 0.6$‰ (1σ) and $\delta^{17}O = 4.7 \pm 0.8$‰ (1σ).

No substantial differences have been observed between the oxygen isotopic composition of olivine and pyroxene (Table 5 and Fig. 4), although pyroxenes tend to show a somewhat larger range in $\delta^{18}O$ and $\delta^{17}O$ than olivine grains (Table 5 and Fig. 4).

Most of the analyzed grains plot between the terrestrial fractionation (TF) line and the carbonaceous chondrite anhydrous minerals (CCAM) line (Clayton et al. 1973). All analyses seem to be well-fitted by the Young and Russell (YR) line (Young and Russell 1998). The displacement from the TF line, expressed as $\Delta^{17}O$, varies from −6.0 to −1.0‰ and from −3.3 to 1.0‰ for crystalline and fine-grained micrometeorites, respectively. The pyroxene belonging to a scoriaceous micrometeorite has $\Delta^{17}O$ within uncertainty of terrestrial (0.3‰ ± 0.9‰). Different grains belonging to the same micrometeorite can have different oxygen isotopic compositions (see Table 5).

DISCUSSION

Comparison with Large AMMs

In order to assess whether or not there might be true differences between micrometeorites of different sizes, it is

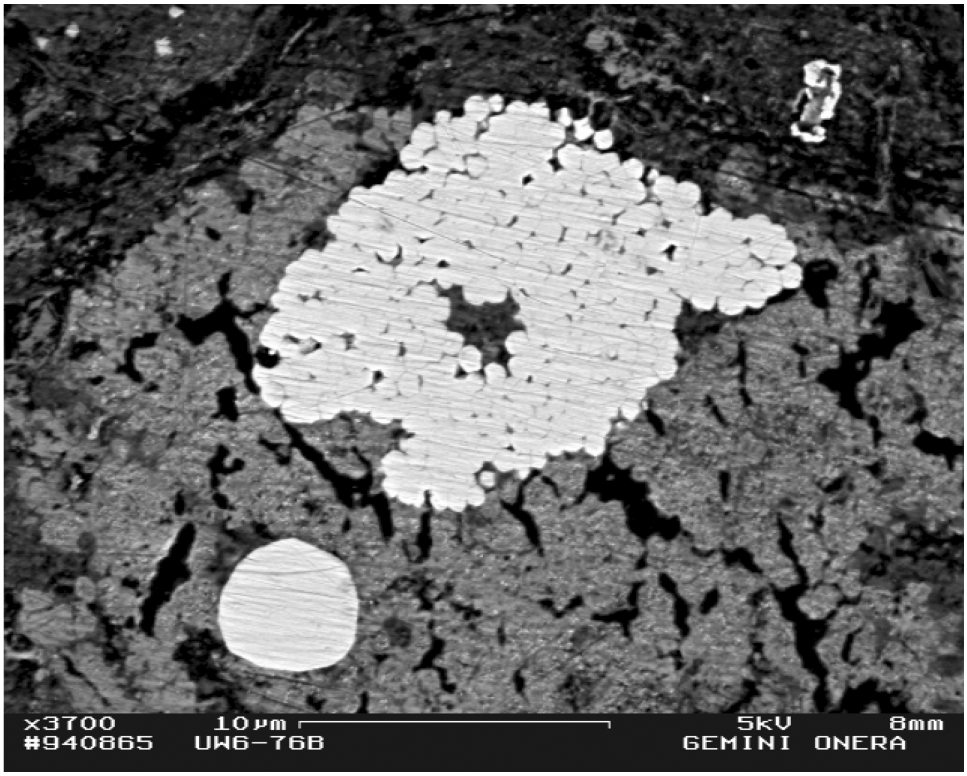

Fig. 3. Backscattered scanning electron image of the interior of a fine-grained micrometeorite. Magnetite framboids are embedded in dehydrated phyllosilicate.

important to first ascertain if AMMs of the 25–50 μm size fraction are true small micrometeorites or mere fragments of a larger size fraction generated during the collection procedure. The presence of a partial to complete magnetite rim on the majority of small micrometeorites (Fig. 1) is a good indicator for the 25–50 μm size fraction AMMs not being fragments of larger micrometeorites. However, this is not a definite criterion, since it depends critically on the sample preparation. Inappropriate polishing might fail to reveal magnetite rims (Toppani et al. 2001). A more reliable criterion is the presence or absence of glassy cosmic spherules. These objects are very fragile, and the presence of one glassy spherule out of seven cosmic spherules is an indication that micrometeorites endure minimum fragmentation during the collection procedure.

Small AMMs (25–50 μm size fraction) do not exhibit unusual textures when compared to the larger AMMs (50–400 μm size fraction): all of the 67 particles studied fall in the four textural groups previously defined by Kurat et al. (1994b). However, the relative abundance of textural types among the small AMMs differs significantly from that of larger AMMs. The unmelted micrometeorites group (fine-grained and crystalline) is by far the dominant population in the 25–50 μm size fraction, whereas larger AMMs display a roughly equal proportion of UMMs and partially melted AMMs (Engrand and Maurette 1998). The UMMs/scoria ratio is ~7 for the 25–50 μm size fraction and ~1 for the 50–400 size fraction (Engrand and Maurette 1998; Kurat et al. 1994b). Similarly, the abundance of cosmic spherules is lower in the small size fraction (10%) compared to the 100–400 μm size fraction (20%) (Engrand and Maurette 1998). These observations suggest that small particles are less heated during atmospheric entry than larger ones, in agreement with atmospheric entry models (Love and Brownlee 1991).

Though the overall chemical compositions of the two populations overlap well (Fig. 2), the bulk chemistry of small micrometeorites present minor differences with the bulk chemistry of large micrometeorites. One scoriaceous small micrometeorite (UW6-29) is conspicuously enriched in magnesium and silicon compared to large micrometeorites. However, this micrometeorite contains a large enstatite grain that displaces its bulk composition toward the enstatite pole (Mg-Si) of the ternary diagram. Two crystalline micrometeorites are also Mg-rich compared to large crystalline micrometeorites. Because enstatite monocrystals are common in the 25–50 μm size fraction, this observation does not constitute an intrinsic difference between small and large AMMs. One fine-grained micrometeorite (UW1-77) has a composition plotting outside the field defined by large micrometeorites (Fig. 2). Cosmic spherules have a wide range of compositions, compatible with that of other Antarctic spherules (Taylor et al. 2000).

Small crystalline AMMs display similar textural and mineralogical characteristics as their larger counterparts.

Table 5. Oxygen isotopic compositions of individual minerals in small AMMs (25–50 μm). Xtal, fg, and sc stand for crystalline, fine-grained, scoriaceous, micrometeorites, respectively. Px and ol stand for pyroxene and olivine, respectively.

Sample	Textural type	Mineral	Mineral composition	$\delta^{18}O$ (‰)[a]	1σ (‰)	$\delta^{17}O$ (‰)[a]	1σ (‰)	$\Delta^{17}O$ (‰)[b]
UW1-12	xtal	px	$En_{97}Wo_0$	–0.9	0.9	–3.0	0.8	–2.5
UW1-44_1	xtal	px	$Ens_{96}Wo_1$	–2.0	1.1	–3.3	0.9	–2.3
UW1-69_1	xtal	px	$En_{98}Wo_1$	0.3	1.4	–3.1	1.3	–3.3
UW3-23	fg	px	$En_{97}Wo_3$	1.0	0.9	–2.8	0.8	–3.3
UW3-4_1	fg	ol	Fo_{97}	1.6	1.1	–0.4	0.9	–1.2
UW3-60	xtal	px	$En_{92}Wo_9$	1.0	0.9	–1.6	0.7	–2.1
UW3-93_1	xtal	px	$En_{94}Wo_2$	0.4	1.1	–0.8	1.0	–1.0
UW6_53_1	fg	px	$En_{99}Wo_1$	–4.1	1.4	–4.9	1.5	–2.8
UW6_53_2	fg	px	$En_{97}Wo_1$	–1.5	1.2	–2.7	1.5	–1.9
UW6_55_1	fg	ol	Fo_{88}	0.6	1.3	0.5	1.4	0.2
UW6_55_2	fg	px	$En_{89}Wo_6$	2.0	1.3	1.7	1.4	0.7
UW6_69_1	xtal	px	$En_{97}Wo_6$	–3.6	1.2	–5.1	1.4	–3.2
UW6_69_2	xtal	ol	Fo_{98}	–4.2	1.6	–6.6	1.4	–4.4
UW6_74_1	xtal	ol	Fo_{90}	–2.4	1.4	–3.2	1.4	–2.0
UW6_85_1	fg	px	$En_{84}Wo_1$	0.6	1.0	0.3	1.0	0.0
UW6_85_2	fg	ol	Fo_{78}	2.5	1.4	2.3	1.6	1.0
UW6-29	sc	px	$En_{99}Wo_0$	8.5	0.6	4.7	0.8	0.3
UW3-56_1	xtal	px	$En_{93}Wo_3$	–11.0	0.9	–11.7	0.7	–6.0
UW3-56_2	xtal	px	$En_{89}Wo_2$	–4.9	1.2	–7.7	0.9	–5.2

[a]Relative to SMOW.
[b]$\Delta^{17}O = \delta^{17}O - 0.52 \times \delta^{18}O$.

Poikilitic and porphyritic textures described by Kurat (1994b) are found in addition to common, irregularly shaped particles. Olivines from small crystalline AMMs compare well to the olivine population described by Kurat et al. (1994b). They have completely overlapping iron contents ($Fo_{64–97}$ compared to $Fo_{63–98}$), compatible FeO/MnO ratios (60–80 compared to 15–130) and similar minor elements contents. Low-Ca pyroxene from the crystalline small AMMs show similar compositional ranges to pyroxene grains from large crystalline AMMs (Beckerling and Bischoff 1995). The iron content of pyroxene studied by Beckerling and Bischoff (1995) peaks at enstatitic compositions comparable to that of pyroxene grains from crystalline small AMMs. In addition, the FeO/MnO ratio in pyroxene from the subset of porphyritic and poikilitic particles analyzed by Beckerling and Bischoff (1995) ranges from 3 to 42 and includes the FeO/MnO range found in our study.

The mineralogy of fine-grained small AMMs is broadly similar to that of their larger counterparts. Relic pyroxene and olivine grains form two distinct compositional groups: an iron-poor group ($Fs_{<6}$ and $Fo_{<3}$, respectively) and an iron-rich group ($Fs_{>16}$ and $Fa_{>18}$, respectively), which have been reported by all AMMs researchers (e.g., Christophe Michel-Lévy and Bourot-Denise 1992; Genge et al. 1997; Kurat et al. 1994b; Steele 1992). The intermediate content of minor elements from relic olivine and pyroxene grains also matches the ranges of similar grains from larger AMMs (Fig. 5). Matrix compositions of fine-grained AMMs match the matrix analyses of phyllosilicate-like phases (Genge et al. 1997; Nakamura et al. 2001; Noguchi et al. 2002). Framboidal magnetite is present in two small fine-grained AMMs. These peculiar magnetite textures being typical of CI carbonaceous chondrites (Jedwab 1967; Kerridge 1970), their presence in an Antarctic micrometeorite has been used by Kurat et al. (1992) to define CI AMMs. These authors report 7 CI AMMs out of 110 UMMs (i.e., an abundance relative to UMMs of ~6%). Among small AMMs, the abundance of framboid-bearing AMMs is ~4% relative to UMMs. This figure is compatible with that of the larger size fraction given the statistical uncertainties due to our (relatively) small number of particles studied. Contrary to large AMMs (Engrand et al. 1999a; Greshake et al. 1996; Hoppe et al. 1995; Kurat et al. 1994a; Kurat et al. 1994c), no calcium-aluminium-rich inclusion (CAI) was found among small AMMs. However, this can easily be explained on statistical grounds, since the abundance of CAIs is ~0.4% in large AMMs (Gounelle 2000). Small AMMs have an average surface that is 10 times smaller than that of large AMMs. Consequently, we should have examined ~1000 small AMMs to expect one single CAI. As we studied only 67 of them, the absence of CAIs in our restricted set of particles is not conclusive.

The texture of scoriaceous small AMMs is identical to that of large scoriaceous AMMs. The mineralogy of scoriaceous small AMMs compares well to that of their larger counterparts. Kurat et al. (1994b) report fayalitic olivine ($Fo_{68–77}$) in scoriaceous particles, the composition of which is close to that of the only olivine we found among scoriaceous small AMMs (Fo_{63}). Pyroxene compositions from small

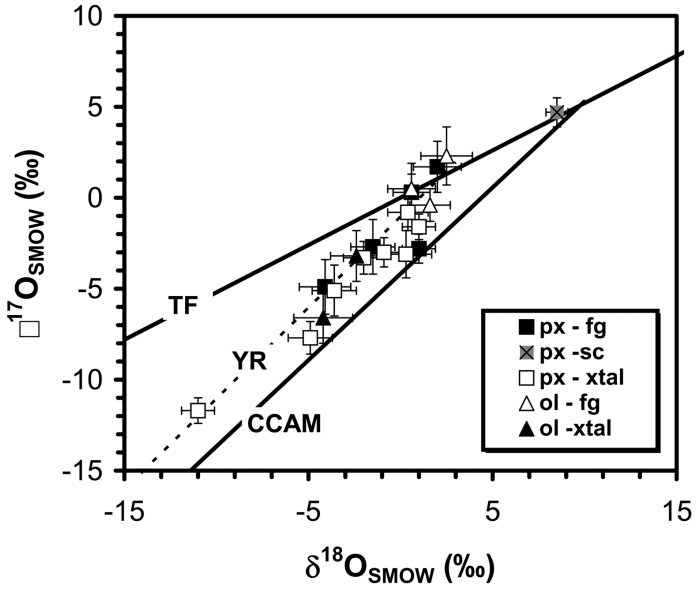

Fig. 4. Three-isotope diagram showing the oxygen isotopic composition of olivine and pyroxene grains belonging to 25–50 μm micrometeorites. The carbonaceous chondrite anhydrous minerals (CCAM) mixing line (Clayton et al. 1973), and the Young and Russell (YR) line (Young and Russell 1998) are shown for reference. Terrestrial samples lie along the terrestrial fractionation (TF) mixing line. Error bars are 1σ.

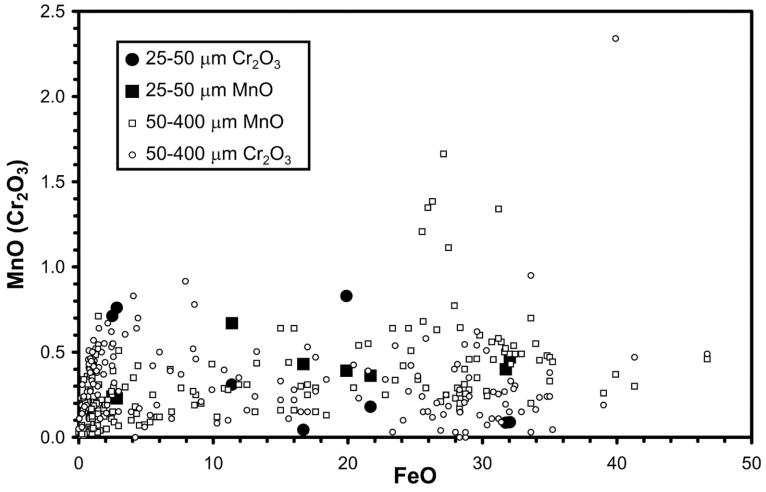

Fig. 5. Minor element contents (wt%) of olivine grains in 25–50 μm micrometeorites (this work) compared to 50–400 μm micrometeorites (data from Orsay and Vienna laboratories).

($En_{99}Wo_0$) and large ($En_{95–99}Wo_{0–1}$) AMMs are likewise similar.

Our cosmic spherule population is too small to meaningfully compare it with the cosmic spherules found in the 50–400 μm size fraction. It is worth noting, however, that all the textures we observe are compatible with the textures described for large Antarctic cosmic spherules (Taylor et al. 2000). In addition, the bulk composition of the 25–50 μm cosmic spherules (Fig. 2) matches that of larger cosmic spherules (Brownlee et al. 1997).

Figure 6 displays the oxygen isotopic composition of pyroxene and olivine grains belonging to small AMMs (this work) together with that of pyroxene and olivine grains belonging to large AMMs (Engrand et al. 1999a). Both populations have similar oxygen isotope systematics. The only minor difference is that in the 25–50 μm size fraction, the most ^{16}O-poor grain is a pyroxene, while in the 50–400 μm size fraction, it is an olivine. Olivine and pyroxene from small and large micrometeorites obviously sample the same oxygen isotopic reservoir.

Engrand et al. (1999c) have measured the hydrogen isotopic composition of six fine-grained and three

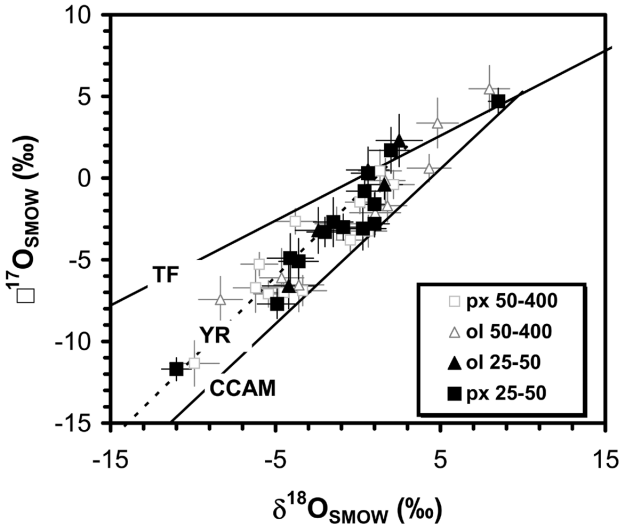

Fig. 6. Three-isotope plot showing the oxygen isotopic composition of olivine and pyroxene grains of the 25–50 μm and 50–400 μm micrometeorites. The carbonaceous chondrite anhydrous minerals (CCAM) mixing line (Clayton et al. 1973), and the Young and Russell (YR) line (Young and Russell 1998) are shown for reference. TF stands for terrestrial fractionation line. Error bars are 1σ.

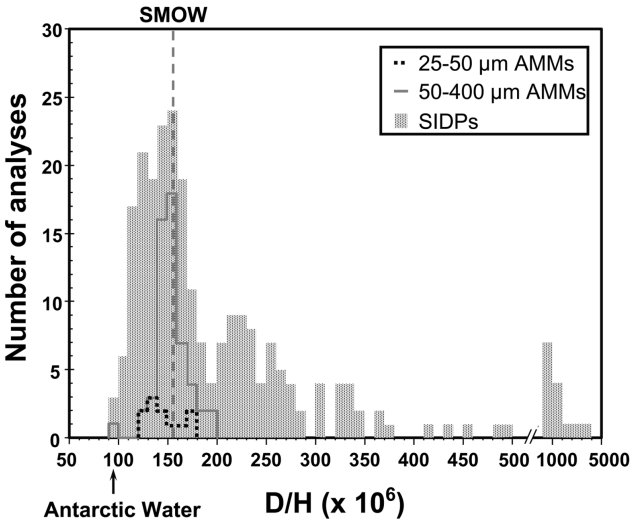

Fig. 7. The hydrogen isotopic composition of small (25–50 μm) AMMs compared to that of large AMMs (100–400 μm) and IDPs. Data from Engrand et al. (1999c) for the AMMs and Zinner et al. (1983), McKeegan et al. (1985), McKeegan (1987), Messenger (1997) for SIDPs.

scoriaceous micrometeorites belonging to the 25–50 μm size fraction (Fig. 7). Small AMMs have D/H ratios comparable to that of the Earth oceans (SMOW), and are similar to that of the large micrometeorites (Engrand et al. 1999c), compatible with a common origin between small and large micrometeorites.

Comparison with IDPs

There are important differences between IDPs and small (25–50 μm) AMMs in term of texture and morphology. The abundance of anhydrous particles among IDPs is higher, varying between 34% (Zolensky and Lindstrom 1992) and 50% (Bradley et al. 1988), compared to an abundance of crystalline micrometeorites among AMMs of 22% (this work). The presence of scoriaceous particles, abundant within the AMMs collection (Table 1) has not been reported within the IDPs collection (Rietmeijer 1998). Magnetite rims, which are common among the small AMMs, are rare among IDPs (Zolensky and Lindstrom 1992). These last two observations suggest that IDPs may have suffered less heating from atmospheric entry than have small AMMs (Keller et al. 1996).

Strong mineralogical differences between small AMMs and IDPs have also been identified. Carbonates in IDPs have been reported by many authors (Thomas et al. 1995; Tomeoka and Buseck 1985; Zolensky and Lindstrom 1992), while we have not found any carbonate among the 67 AMMs studied. Likewise, iron-nickel sulfides such as pyrrhotite and pentlandite have been reported to be abundant in IDPs (Dai and Bradley 2001; Thomas et al. 1995; Zolensky and Lindstrom 1992; Zolensky and Thomas 1995), while we found only two iron-nickel sulfide grains in the course of our study. Finally, low-iron-manganese-enriched (LIME) olivines (FeO/MnO < 1), ubiquitous in IDPs (Klöck et al. 1989), are absent from the small AMMs studied.

A key difference between IDPs and small micrometeorites concern the hydrogen isotope composition. Porous anhydrous cluster IDPs often exhibit large isotopic anomalies in hydrogen (e.g., Messenger 2000) that have not been found in the small size fraction of AMMs (Engrand et al. 1999c). Exchange and contamination experiments performed by Engrand et al. (1999c) have demonstrated that the terrestrial hydrogen isotopic composition of AMMs is not the result of exchange during the 50,000 year sojourn of AMMs within blue ice, or the 8 hour exposition to melted ice during recovery. The distinct hydrogen isotopic composition of AMMs and IDPs is therefore not due to the prolonged stay of AMMs within Antarctic ice, but has some other cause. It is possible that the difference arises from using different analytical techniques. Engrand et al. (1999c) used an O^- beam to measure the isotopic composition of hydrogen in AMMs, while a Cs^+ beam was used to characterize the hydrogen isotopic composition of IDPs (e.g., Messenger 2000; Mukhopadhyay and Nittler 2003). Deloule and Robert (1995) demonstrated that an O^- beam enhances the emission of H^+ ions from the H-bearing silicate phases over that of organic H^+ ions by a factor of >100 (cf. Gounelle et al. 2005), while transmission electron microscope studies performed by Keller et al. (2004) indicate that the D-rich matter in IDPs is organic. An exception are two cluster IDPs studied by Mukhopadhyay and Nittler (2003), which exhibit D-rich water. The apparent difference in hydrogen isotopic

composition between AMMs and IDPs could be in part due to a difference in the analytical techniques.

Although there has been recently a growing interest in measuring the oxygen isotopic composition of IDPs using ion probe imaging techniques (e.g., Aléon et al. 2001; Floss and Stadermann 2003; Messenger 1998; Messenger 1999), there have been relatively few ion probe studies on the oxygen isotopic composition of individual anhydrous grains in IDPs. Most of them are dedicated to refractory minerals such as spinel, corundum, or melilite (e.g., Greshake et al. 1996; McKeegan 1987). Engrand et al. (1999b) measured the oxygen isotopic composition of olivine and pyroxene in four IDPs. Seven analyses plot in the same field as AMMs in a three oxygen isotopes plot (Engrand et al. 1999b). One analysis—corresponding to a GEMs-rich particle—exhibits an enrichment in ^{16}O with $\delta^{18}O = -19.7 \pm 1.6$ (1σ) and $\delta^{17}O = -19.5 \pm 1.8‰$ (1σ). No similar enrichment has been discovered in small AMMs (this study). The only ^{16}O enrichments found so far in AMMs correspond to refractory minerals such as melilite and spinel (Engrand et al. 1999a; Hoppe et al. 1995; Kurat et al. 1994c). Messenger et al. (2003) have discovered recently very large oxygen isotope anomalies in six silicate grains using the NanoSIMS. Because of their rarity (6 out of 1031) and their small size, these circumstellar grains would not have been discovered using a conventional ion microprobe. Using similar techniques, Yada et al. (2004) have discovered a large (5 × 3 μm) presolar silicate in an AMM collected in Cap Prudhomme in 1988 (Maurette et al. 1991).

Although small AMMs bridge the size gap between large AMMs (>50 μm) and IDPs (<50 μm), only a small population of IDPs has sizes larger than 25 μm. Most of them are the so-called cluster IDPs that are often the bearers of the largest isotopic anomalies (e.g., Rietmeijer 1998). Most of the above comparisons between AMMs and IDPs are based on cluster IDPs, while comparison with noncluster IDPs implicitly assumes that there is a continuum between cluster and noncluster IDPs. In any case, comparing AMMs with sizes below 50 μm and IDPs establishes textural, morphological, mineralogical, and isotopic differences between these populations. Because the size of the samples studied overlap, the differences between AMMs and IDPs are not due to a size effect, but have other causes that we will outline in the next section.

CONCLUSIONS

We have investigated the texture, bulk chemistry, mineralogy, as well as the anhydrous grains oxygen isotopic composition of 67 micrometeorites collected at Cap Prudhomme, Antarctica and belonging to the size fraction 25–50 μm (small AMMs). Small AMMs can be classified in the same four textural classes as large AMMs (>100 μm) (Kurat et al. 1994b): crystalline, fine-grained, scoriaceous, and cosmic spherules. Bulk compositions of the major elements Fe, Mg, and Si show no striking differences with those of large micrometeorites. The mineralogy of a given textural class of small AMMs also compares well to that of large AMMs of the same textural class. Similarly, the oxygen isotopic compositions of olivine and pyroxene grains of small AMMs overlap those of large AMMs. Engrand et al. (1999c) had also shown that phyllosilicate water in both small and large AMMs had similar hydrogen isotopic compositions. To summarize, small AMMs (25–50 μm) strongly resemble larger AMMs (50–400 μm) in terms of texture, mineralogy, and isotopic composition. The AMMs population is thus compositionally homogeneous over the size range 25–400 μm. There is no change of the composition of the micrometeorite flux with size.

Small AMMs overlap in size with the largest IDPs and therefore can be directly compared to this other population of micrometeorites. Here we find that differences do exist between small AMMs and IDPs, especially in terms of texture and mineralogy. Minerals such as carbonates and iron-nickel sulfides, abundant within the IDPs, are not found in the small AMMs. The main difference, however, is the absence within the AMMs population of anhydrous, porous particles often exhibiting large isotopic anomalies in hydrogen and oxygen (Messenger 2000; Messenger et al. 2003). Because the sizes of small AMMs and IDPs overlap, the observed differences are not due to a size effect, but have other causes, such as physical biases introduced during collection techniques or a temporal variation in the composition of the micrometeorite flux.

A recent temporal change in the composition of the micrometeorite flux could explain the differences observed between AMMs and IDPs, since Cap Prudhomme micrometeorites sample the flux ~50,000 years ago (Maurette et al. 1994), while IDPs sample the present micrometeorite flux. A recent temporal change in the composition of the micrometeorite flux onto Earth is however difficult to assess. To establish such a change, one would need to collect 50,000-year-old micrometeorites with a technique that introduces biases similar to that of stratospheric collections. This seems difficult to achieve at the present time.

Assessing the biases introduced by the collection procedures in Antarctica and elsewhere is an important task for micrometeorites researchers (e.g., Duprat et al. 2003; Gounelle 2000; Maurette et al. 1994; Taylor et al. 1998). First, because micrometeorites are key samples for understanding the origin and evolution of the solar system, we want to have the most precise picture of the true population of micrometeorites accreting to Earth. Second, the determination of the micrometeorite mass flux onto Earth relies on a good collection efficiency and the minimization of the biases (Duprat et al. 2001; Gounelle 2000).

Physical biases can be due to the preferential destruction of certain particle types during collection procedures. For

example, it is likely that the pumps used in the Antarctic blue ice micrometeorites collections (Maurette et al. 1994) destroy the most friable particles found in the IDPs collection, such as the chondritic porous particles. Conversely, it is possible that hard particles, such as scoriaceous or crystalline micrometeorites, stick less efficiently to the silicon oil collectors used in stratospheric collections than the porous particles. The interaction of the terrestrial environment with micrometeorites can also introduce significant biases in the collection of micrometeorites. Some IDPs are known to be enriched in bromine relative to chondritic values (Rietmeijer 1998), which is indicative of possible atmospheric contamination. The absence of carbonates in Antarctic micrometeorites has been interpreted as resulting from the residence of micrometeorites with melt water, which might promote the dissolution of carbonates.

In the future, it is of outmost importance to develop micrometeorite collection procedures that minimize physical biases. In January 2002, Duprat et al. (2003) conducted a field trip in the central regions of Antarctica, at the station CONCORDIA (Dome C, S75° E123°). Because they collected micrometeorites in surface snow rather than in blue ice, and because they developed a procedure that does not involve mechanical pumping, the CONCORDIA collection may provide the most unbiased collection of Antarctic micrometeorites that can be compared to the stratospheric collection.

Acknowledgments–Dr. Mireille Christophe-Michel Lévy provided insightful comments. Mr. Boivin helped with the FEG-SEM kindly made available by ONERA (Chatillon, France). Drs. Theo Naftlos and Michel Fialin kindly helped with the EMP analyses in Vienna and Paris. The two reviewers, Drs. Larry Nittler and Mike Zolensky, as well as the associate editor, Dr. Scott Sandford, helped in improving the paper. We thank the IPEV, CNES, PNP and IN2P3 for continuous support. The UCLA ion microprobe laboratory is supported by grants from the NASA Cosmochemistry program and the Instrumentation and Facilities program of the NSF. This work was part of the Ph.D. thesis of M.G.

Editorial Handling—Dr. Scott Sanford

REFERENCES

Aléon J., Engrand C., Robert F., and Chaussidon M. 2001. Clues to the origin of interplanetary dust particles from the isotopic study of their hydrogen-bearing phases. *Geochimica et Cosmochimica Acta* 65:4399–4412.

Beckerling W. and Bischoff A. 1995. Occurence and composition of relict minerals in micrometeorites from Greenland and Antartica. Implications for their origins. *Planetary and Space Science* 43: 435–449.

Bradley J. P. 1994. Chemically anomalous preaccretionally irradiated grains in interplanetary dust from comets. *Science* 265:925–929.

Bradley J. P., Sandford S. A., and Walker R. M. 1988. Interplanetary dust. In *Meteorites and the early solar system*, edited by Kerridge J. F. and Matthews M. S. Tucson, Arizona: The University of Arizona Press. pp. 861–895.

Bradley J. P., Keller L. P., Snow T. P., Hanner M. S., Flynn G. J., Gezo J. C., Clemett S. J., Brownlee D. E., and Bowey J. E. 1999. An infrared spectral match between GEMS and interstellar grains. *Science* 285:1716–1718.

Brownlee D. E. 1985. Cosmic dust: Collection and research. *Annual Review of Earth and Planetary Sciences* 13:147–173.

Brownlee D. E., Bates B., and Schramm L. 1997. The elemental composition of stony cosmic spherules. *Meteoritics & Planetary Science* 32:157–175.

Christophe Michel-Lévy M. and Bourot-Denise M. 1992. Mineral composition in Antarctic and Greenland micrometeorites. *Meteoritics* 27:73–80.

Clayton R. N., Grossman L., and Mayeda T. K. 1973. A component of primitive nuclear composition in carbonaceous meteorites. *Science* 182:485–488.

Dai Z. R. and Bradley J. P. 2001. Iron-nickel sulfides in anhydrous interplanetary particles. *Geochimica et Cosmochimica Acta* 65: 3601–3612.

Deloule E. and Robert F. 1995. Interstellar water in meteorites? *Geochimica et Cosmochimica Acta* 59:4695–4706.

Duprat J., Engrand C., Maurette M., Gounelle M., Hammer C., and Kurat G. 2003. The CONCORDIA-collection: Pristine contemporary micrometeorites from central Antarctica surface snow (abstract #1727). 34th Lunar and Planetary Science Conference. CD-ROM.

Duprat J., Maurette M., Engrand C., Matrajt G., Immel G., Gounelle M., and Kurat G. 2001. An estimation of the contemporary micrometeorite flux obtained from surface snow samples collected in central Antarctica (abstract). *Meteoritics & Planetary Science* 36:A52.

Engrand C. and Maurette M. 1998. Carbonaceous micrometeorites from Antarctica. *Meteoritics & Planetary Science* 33:565–580.

Engrand C., McKeegan K. D., and Leshin L. A. 1999a. Oxygen isotopic compositions of individual minerals in Antarctic micrometeorites: Further links to carbonaceous chondrites. *Geochimica et Cosmochimica Acta* 63:2623–2636.

Engrand C., McKeegan K. D., Leshin L. A., Bradley J. P., and Brownlee D. E. 1999b. Oxygen isotopic compositions of interplanetary dust particles: ^{16}O-excess in a GEMS-rich IDP (abstract #1690). 30th Lunar and Planetary Science Conference. CD-ROM.

Engrand C., Deloule E., Robert F., Maurette M., and Kurat G. 1999c. Extraterrestrial water in micrometeorites and cosmic spherules from Antarctica: An ion microprobe study. *Meteoritics & Planetary Science* 34:773–787.

Floss C. and Stadermann F. J. 2003. Complementary carbon, nitrogen and oxygen isotopic imaging of interplanetary dust particles: Presolar grains and an indication of a carbon isotopic anomaly (abstract #1238). 34th Lunar and Planetary Science Conference. CD-ROM.

Genge M. J., Grady M. M., and Hutchison R. H. 1997. The textures and compositions of fine-grained micrometeorites: Implications for comparisons with meteorites. *Geochimica et Cosmochimica Acta* 61:5149–5162.

Gounelle M. 2000. Matière extraterrestre sur Terre: Des Océans aux protoétoiles. Ph.D. thesis, Université Paris, Paris, France.

Gounelle M., Maurette M., Engrand C., Brandstätter F., and Kurat G. 1999. Mineralogy of the 1998 Astrolabe Antarctic micrometeorite collection (abstract). *Meteoritics & Planetary Science* 34:A46.

Gounelle M., Engrand C., Alard O., Bland P. A., Zolensky M. E., Russell S. S., and Duprat J. Forthcoming. The hydrogen isotopic

composition of water from fossil micrometeorites. *Geochimica et Cosmochimica Acta*.

Greshake A., Hoppe P., and Bischoff A. 1996. Mineralogy, chemistry, and oxygen isotopes of refractory inclusions from stratospheric interplanetary dust particles and micrometeorites. *Meteoritics & Planetary Science* 31:739–748.

Hoppe P., Kurat G., Walter J., and Maurette M. 1995. Trace elements and oxygen isotopes in a CAI-bearing micrometeorite from Antarctica (abstract). 26th Lunar and Planetary Science Conference. pp. 623–624.

Jedwab J. 1967. La météorite en plaquettes des météorites carbonées d'Alais, Ivuna et Orgueil. *Earth and Planetary Science Letters* 2: 440–444.

Keller L. P., Thomas K. L., and McKay D. S. 1996. Mineralogical changes in IDPs resulting from atmospheric entry heating. In *Physics, chemistry, and dynamics of interplanetary dust*, vol. 104, edited by Gustafson B. S. and Hanner M. S. pp. 295–298.

Keller L. P., Messenger S., Flynn G. J., Clemett S. J., Wirick S., and Jacobsen C. 2004. The nature of molecular cloud material in interplanetary dust. *Geochimica et Cosmochimica Acta* 68:2577–2589.

Kerridge J. F. 1970. Some observations on the nature of magnetite in the Orgueil meteorite. *Earth and Planetary Science Letters* 9: 299–306.

Klöck W., Thomas K. L., McKay D. S., and Palme H. 1989. Unusual olivine and pyroxene composition in interplanetary dust and unequilibrated ordinary chondrite. *Nature* 339:126–128.

Kortenkamp S. J., Dermott S. F., Fogle D., and Grogan K. 2001. Sources and orbital evolution of interplanetary dust accreted by the Earth. In *Accretion of extraterrestrial matter throughout Earth's history*, edited by Peucker-Eherenbrink B. and Schmitz B. Kluwer/Plenum: New York. pp. 13–30.

Kurat G., Presper T., Brandstätter F., Maurette M., and Koeberl C. 1992. CI-like micrometeorites from Cap-Prudhomme, Antarctica (abstract). 23rd Lunar and Planetary Science Conference. pp. 747–748.

Kurat G., Hoppe P., and Maurette M. 1994a. Preliminary report on spinel-rich CAIs in an Antarctic micrometeorite (abstract). 25th Lunar and Planetary Science Conference. pp. 763–764.

Kurat G., Koeberl C., Presper T., Brandstätter F., and Maurette M. 1994b. Petrology and geochemistry of Antarctic micrometeorites. *Geochimica et Cosmochimica Acta* 58:3879–3904.

Kurat G., Hoppe P., Walter J., Engrand C., and Maurette M. 1994c. Oxygen isotopes in spinels from Antarctic micrometeorites (abstract). *Meteoritics* 29:487–488.

Love S. G. and Brownlee D. E. 1991. Heating and thermal transformation of micrometeoroids entering the Earth's atmosphere. *Icarus* 89:26–43.

Love S. G. and Brownlee D. E. 1993. A direct measurement of the terrestrial mass accretion rate of cosmic dust. *Science* 262:550–553.

Maurette M., Pourchet M., and Perreau M. 1992a. The 1991 EUROMET micrometeorite collection at Cap-Prudhomme, Antarctica. *Meteoritics* 27:473–475.

Maurette M., Brownlee D. E., Joswiak D. J., and Sutton S. R. 1992b. Antarctic micrometeorites smaller than 50 microns (abstract). 23rd Lunar and Planetary Science Conference. pp. 857–858.

Maurette M., Hammer C., Brownlee D. E., Reeh N., and Thomsen H. H. 1986. Placers of cosmic dust in the blue ice lakes of Greenland. *Science* 233:869–872.

Maurette M., Immel G., Hammer C., Harvey R., Kurat G., and Taylor S. 1994. Collection and curation of IDPs from the Greenland and Antarctic ice sheets. In *Analysis of interplanetary dust,* vol. 310, edited by Zolensky M. E., Wilson T. L., Rietmeijer F. J. M., and Flynn G. J. Houston: American Institute of Physics. pp. 277–289.

Maurette M., Olinger C., Christophe Michel-Lévy M., Kurat G., Pourchet M., Brandstätter F., and Bourot-Denise M. 1991. A collection of diverse micrometeorites recovered from 100 tons of Antarctic blue ice. *Nature* 351:44–47.

McKeegan K. D. 1987. Oxygen isotopes in refractory stratospheric dust particles: Proof of extraterrestrial origin. *Science* 237:1468–1471.

Messenger S. 1998. Oxygen isotopic imaging of interplanetary dust (abstract). *Meteoritics & Planetary Science* 33:A106.

Messenger S. 1999. Oxygen isotopic imaging of interplanetary dust by TOF-SIMS (abstract #1600). 29th Lunar and Planetary Science Conference. CD-ROM.

Messenger S. 2000. Identification of molecular-cloud material in interplanetary dust particles. *Nature* 404:968–971.

Messenger S., Keller L. P., Stadermann F. J., Walker R. J., and Zinner E. 2003. Samples of stars beyond the solar system: Silicate grains in interplanetary dust. *Science* 300:105–108.

Mukhopadhyay S. and Nittler L. R. 2003. D-rich water in interplanetary dust particles (abstract #1941). 34th Lunar and Planetary Science Conference. CD-ROM.

Nakamura T., Noguchi T., Yada T., Nakamuta Y., and Takaoka N. 2001. Bulk mineralogy of individual micrometeorites determined by X-ray diffraction analysis and transmission electron microscopy. *Geochimica et Cosmochimica Acta* 65: 4385–4397.

Nakamura T., Imae N., Nakai I., Noguchi T., Yano H., Terada K., Murakami T., Fukuoka T., Nogami K.-I., Ohashi H., Nozaki W., Hashimoto M., Kondo N., Matsuzaki H., Ichikawa O., and Ohmori R. 1999. Antarctic micrometeorites collected at the Dome Fuji Station. *Antarctic Meteorite Research* 12:183–198.

Noguchi T., Nakamura T., and Nozaki W. 2002. Mineralogy of phyllosilicate-rich micrometeorites and comparison with Tagish Lake and Sayama meteorites. *Earth and Planetary Science Letters* 202:229–246.

Rietmeijer F. J. M. 1998. Interplanetary dust particles. In *Planetary materials*, edited by Papike J. J. Washington, D.C.: Mineralogical Society of America. pp. 2-1–2-94.

Steele I. M. 1992. Olivine in Antarctic micrometeorites: Comparison with other extraterrestrial olivine. *Geochimica et Cosmochimica Acta* 56:2923–2929.

Taylor S., Lever J. H., and Harvey R. P. 1998. Accretion rate of cosmic spherules measured at South Pole. *Science* 392:899–903.

Taylor S., Lever J. H., and Harvey R. P. 2000. Numbers, types and compositions of an unbiased collection of cosmic spherules. *Meteoritics & Planetary Science* 35:651–666.

Terada K., Yada T., Kojima H., Noguchi T., Nakamura T., Murakami T., Yano H., Nozaki W., Nakamuta Y., Matsumoto N., Kamata J., Mori T., Nakai I., Sasaki M., Itabashi M., Setoyanagi T., Nagao K., Osawa T., Hiyagon H., Mizutani S., Fukuoka T., Nogami K.-I., Ohmori R., and Ohashi H. 2001. General characterization of Antarctic micrometeorites collected by the 39th Japanese Antarctic Research Expedition: Consortium studies of JARE AMMs (II). *Antarctic Meteorite Research* 14: 89–107.

Thomas K. L., Blandford G. E., Clemett S. J., Flynn G. J., Keller L. P., Klöck W., Maechling C. R., McKay D. S., Messenger S., Nier A. O., Schlutter D. J., Sutton S. R., Warren J. L., and Zare R. N. 1995. An asteroidal breccia: The anatomy of a cluster IDP. *Geochimica et Cosmochimica Acta* 59:2797–2815.

Tomeoka K. and Buseck P. R. 1985. Hydrated interplanetary dust particle linked with carbonaceous chondrites? *Nature* 314:338–340.

Toppani A., Libourel G., Engrand C., and Maurette M. 2001.

Experimental simulation of atmospheric entry of micrometeorites. *Meteoritics & Planetary Science* 36:1377–1396.

Vokrouhlicky D. and Farinella P. 2000. Efficient delivery of meteorites to the Earth from a wide range of asteroid parent bodies. *Nature* 407:606–608.

Warren J. L. and Zolensky M. E. 1994. Collection and curation of interplanetary dust particles recovered from the stratosphere by NASA. In *Analysis of interplanetary dust*, edited by Zolensky M. E., Wilson T. L., Rietmeijer F. J. M., and Flynn G. J. Houston: American Institute of Physics. pp. 245–253.

Yada T., Stadermann F. J., Floss C., Zinner E., and Olinger C. T. 2004. First presolar silicate discovered in an Antarctic micrometeorite (abstract #9056). Workshop on Chondrites and Protoplanetary Disk. CD-ROM.

Young E. D. and Russell S. S. 1998. Oxygen reservoirs in the early solar nebula inferred from an Allende CAI. *Science* 282:452–455.

Zolensky M. E. and Lindstrom D. J. 1992. Mineralogy of 12 large "chondritic" interplanetary dust particles. Proceedings, 22nd Lunar and Planetary Science Conference. pp. 161–169.

Zolensky M. E. and Thomas K. L. 1995. Iron and iron-nickel sulfides in chondritic interplanetary dust particles. *Geochimica et Cosmochimica Acta* 59:4707–4712.

APPENDIX

Appendix 1. Bulk analyses of micrometeorites belonging to the 25–50 μm size fraction. Data in wt%. Xtal, fg, and sc stand for crystalline, fine-grained, and scoriaceous micrometeorites, respectively. B.d. stands for below detection limit.

Micrometeorite	UW6-69	UW1-12	UW6-53	UW5-95	UW1-66	UW1-28	UW6-9	UW6-29	UW1-6
Textural type	xtal	xtal	xtal	cs	cs	cs	sc	sc	sc
SiO_2	46.8	54.1	46.4	33.4	33.2	12.2	23.0	56.6	21.8
TiO_2	0.10	0.07	0.06	0.10	0.10	0.13	0.07	0.05	0.05
Al_2O_3	1.24	0.34	1.09	2.49	0.98	5.05	3.01	3.60	2.89
Cr_2O_3	0.80	0.63	0.65	0.31	0.61	2.57	0.31	0.26	0.45
FeO	8.29	1.96	14.6	29.6	33.2	53.8	30.0	1.66	30.4
MnO	0.16	0.14	0.12	0.25	0.23	0.23	0.23	0.09	0.23
MgO	38.3	34.0	38.6	22.9	26.0	9.30	14.6	31.4	17.0
NiO	0.17	b.d.	0.65	0.72	b.d.	0.20	0.21	b.d.	0.23
CaO	0.60	0.30	0.76	1.26	0.49	0.15	0.36	0.44	0.44
Na_2O	0.07	b.d.	0.03	0.03	0.04	0.19	0.21	0.33	0.25
K_2O	b.d.	b.d.	b.d.	b.d.	0.04	0.07	0.10	0.16	0.06
S	0.10	b.d.	0.04	b.d.	0.03	0.17	0.23	0.11	0.80
Total	96.51	91.54	102.97	91.05	94.88	83.89	72.09	94.60	73.80

Micrometeorite	UW1-64	UW1-68	UW5-92	UW6-77	UW6-55	UW6-88	UW5-11	UW5-25	UW5-62
Textural type	fg	fg	fg	fg	fg	fg	fg	fg	fg
SiO_2	45.1	36.9	21.4	15.3	39.2	35.0	32.6	33.9	28.3
TiO_2	0.03	b.d.	0.05	b.d.	0.09	0.14	0.14	0.07	0.05
Al_2O_3	b.d.	0.03	1.68	1.03	6.98	5.36	2.49	2.84	2.04
Cr_2O_3	0.76	0.97	0.26	0.38	0.84	0.53	0.57	0.34	0.35
FeO	17.5	3.52	20.3	54.9	12.0	32.3	28.9	24.9	27.4
MnO	0.40	0.12	0.17	0.27	0.50	0.38	0.56	0.10	0.24
MgO	29.4	43.7	14.5	1.95	26.0	20.1	15.1	16.2	15.8
NiO	b.d.	b.d.	0.11	0.03	0.11	b.d.	0.44	0.15	0.30
CaO	b.d.	0.06	0.35	0.20	1.17	1.44	1.52	0.37	0.57
Na_2O	0.09	0.20	0.74	0.35	0.04	b.d.	0.25	0.09	0.24
K_2O	0.03	b.d.	0.43	0.27	b.d.	0.09	0.15	0.13	0.05
S	b.d.	b.d.	0.32	0.54	0.10	0.06	0.65	0.51	0.39
Total	93.31	85.49	59.99	74.67	86.93	95.34	82.73	79.08	75.34

Micrometeorite	UW5-78	UW5-85	UW5-96	UW5-97	UW5-104	UW6-12	UW6-18	UW6-43	UW6-76	UW1-74
Textural type	fg	fg	fg	fg	fg	fg	fg	fg	fg	fg
SiO_2	25.0	30.4	30.0	31.3	26.5	20.5	32.6	33.9	29.6	34.7
TiO_2	0.10	0.06	0.12	0.13	0.12	0.11	0.08	0.10	0.07	0.10
Al_2O_3	2.47	2.04	1.88	2.23	1.94	1.48	3.57	2.17	2.74	2.20
Cr_2O_3	0.33	0.31	0.65	0.41	0.42	0.39	0.60	0.49	0.44	0.60
FeO	31.4	16.3	29.3	24.9	31.4	32.6	28.9	20.6	27.9	25.9
MnO	0.19	0.29	b.d.	0.21	0.15	0.22	0.31	0.27	0.25	0.38

Appendix 1. *Continued.* Bulk analyses of micrometeorites belonging to the 25–50 μm size fraction. Data in wt%. Xtal, fg, and sc stand for crystalline, fine-grained, and scoriaceous micrometeorites, respectively. B.d. stands for below detection limit.

Micrometeorite	UW6-69	UW1-12	UW6-53	UW5-95	UW1-66	UW1-28	UW6-9	UW6-29	UW1-6	
MgO	12.2	19.2	5.16	14.5	9.93	9.68	19.2	18.0	17.7	15.4
NiO	0.78	0.43	0.05	0.23	0.23	0.58	0.22	0.53	0.65	0.16
CaO	0.52	1.36	0.31	0.86	0.39	0.47	0.96	0.29	0.12	0.98
Na_2O	0.15	1.86	0.47	0.72	0.43	0.97	0.10	0.92	0.37	0.69
K_2O	0.08	0.25	0.45	0.43	0.11	0.13	0.05	0.13	0.27	0.16
S	0.79	3.11	0.89	0.48	1.13	0.53	0.28	3.59	1.63	0.78
Total	73.21	72.50	68.39	75.91	71.62	67.13	86.59	77.40	80.10	81.27
Micrometeorite	UW6-82	UW6-83	UW6-85	UW6-87	UW6-95	UW6-108	UW1-3	UW1-5	UW1-8	UW1-62
Textural type	fg	fg	fg	fg	fg	fg	fg	fg	fg	fg
SiO_2	35.1	28.6	33.4	33.7	25.7	19.1	29.9	38.3	33.1	38.4
TiO_2	0.12	0.15	0.06	0.07	0.11	0.09	0.13	0.14	0.03	0.15
Al_2O_3	2.37	2.47	2.30	1.78	1.84	1.43	2.65	3.24	3.11	2.58
Cr_2O_3	0.71	0.43	0.48	0.14	0.47	0.41	0.29	0.63	0.37	0.62
FeO	22.70	30.30	22.90	28.90	19.60	25.00	34.50	21.70	30.20	26.20
MnO	0.26	0.21	0.34	0.32	0.08	0.20	0.23	0.13	0.27	0.20
MgO	25.20	17.10	18.80	24.60	11.30	13.60	15.20	17.40	16.60	17.90
NiO	0.17	0.09	0.24	0.46	0.05	0.11	0.21	0.14	0.39	0.17
CaO	0.22	0.21	0.88	1.00	0.06	0.41	0.81	0.43	0.35	0.43
Na_2O	0.23	0.33	0.82	0.28	0.51	0.26	0.28	0.58	0.70	0.69
K_2O	0.06	0.14	0.14	0.06	0.12	0.06	0.17	0.24	0.19	0.14
S	0.26	0.21	0.82	0.45	0.35	0.31	0.35	0.51	1.14	0.75
Total	87.13	80.04	80.37	91.31	59.84	60.66	84.37	82.93	85.31	87.48